

# APPROACHING REIONIZATION: THE EVOLUTION OF THE LYMAN ALPHA FOREST FROM REDSHIFTS FOUR TO SIX

ANTOINETTE SONGAILA<sup>1</sup> & LENNOX L. COWIE<sup>1</sup>

Institute for Astronomy, University of Hawaii, 2680 Woodlawn Drive, Honolulu, HI 96822

*Astronomical Journal, in press (May 2002)*

## ABSTRACT

We analyze the Ly $\alpha$  forest properties of a sample of 15 high redshift quasars lying between  $z = 4.42$  and  $z = 5.75$ , using high signal-to-noise spectra obtained with ESI on the Keck II 10 m telescope. The distribution of transmissions in the Ly $\alpha$  region in this redshift range is shown to be consistent with that found in lambda cold dark matter simulations with a smoothly evolving ionization rate as a function of redshift. The extrapolation of the ionizing flux to  $z = 6.05$  lies a factor of two higher than a  $2\sigma$  upper limit placed by Cen & McDonald (2001) at this redshift, based on the Becker et al. (2001) spectra of the  $z = 6.28$  quasar SDSS 1030+0524. However, the data are also consistent with models in which there is substantial variation of the ionization parameter about the mean value, and in this case, dark gaps such as those seen by Becker et al. become much more likely. We conclude that further data are needed before we can be sure that we have seen the epoch of reionization. We also summarize the damped Ly $\alpha$  systems seen in these quasar lines of sight and measure their metallicities and kinematic properties. We argue that the mean DLA metallicity has dropped substantially by  $z = 5$  compared with its value at  $z < 4$ .

*Subject headings:* early universe — intergalactic medium — quasars: absorption lines — galaxies: formation

## 1. INTRODUCTION

The epoch of reionization marks a fundamental change in the intergalactic gas in which, as the ionized underdense regions merge and overdense regions become exposed to the combined ionizing flux of all the galaxies and AGN, the gas transits from being predominantly neutral to being predominantly ionized over a relatively short redshift interval (e.g. Razoumov et al. 2001, who find  $\Delta z \sim 0.3$ ). As surveys for high  $z$  objects have proceeded rapidly in the last two years, we are approaching redshifts at which the effects of reionization on the IGM might be expected to be becoming apparent. The current highest redshift object is the  $z = 6.56$  Ly $\alpha$  emitter found by Hu et al. (2001) who argue that this object suggests that reionization lies beyond  $z = 6.6$ .

Of more interest for studying the *details* of the intergalactic gas are the extremely luminous quasars being found by the Sloan digital Sky Survey (SDSS) out to a redshift of 6.28 at the present time (e.g. Fan et al. 2001a and references therein). In recent papers, Djorgovski et al. (2001) and Becker et al. (2001) (see also Pentericci et al. 2001 and Fan et al. 2001b) have presented evidence from medium-resolution spectra of the highest redshift SDSS quasars that they claim supports the low redshift edge of reionization at  $z \sim 6$ . There are a number of limitations in both analyses, largely stemming from the small redshift baselines in both cases. Djorgovski et al. used high-quality KeckI LRIS and KeckII ESI spectra of the  $z_{\text{em}} = 5.75$  quasar SDSS 1044–0125 to suggest that they had seen the onset of the ‘trailing edge of the reionization era’ at  $z \sim 5.5$ , based on the presence of opacity gaps in their spectrum blueward of Ly $\alpha$  emission. Becker et al. presented relatively low signal-to-noise spectra of the four highest redshift SDSS quasars and concluded that there is rapid evolution of the mean absorption at these redshifts, including SDSS 1030+0524 with  $z_{\text{em}} = 6.28$ , in which they claimed to see a complete Gunn-Peterson trough at the longest wavelengths observed.

As Becker et al. correctly point out, the appearance of a single Gunn-Peterson trough over a short wavelength interval is not in itself conclusive evidence that the epoch of reionization has been reached since only a small fraction of neutral hydrogen can cause this. The crucial diagnostic of reionization is the evolution of the ionizing flux (cf. Fan et al. 2001b; McDonald & Miralda-Escudé 2001), and for these purposes, a longer redshift baseline is important to deconvolve the effects of the structural thickening of the forest from the ionizing radiation evolution. In this paper we present such a discussion based on ESI spectra of 15 quasars with  $4.42 < z_{\text{em}} < 5.745$ , all of which have a quality comparable to or better than Djorgovski et al.’s spectrum of SDSS 1044–0125, and all of which have highly optimised sky subtraction, a crucial point at the low transmitted flux levels characteristic of these redshifts. The transmitted flux presents a smooth evolution to a redshift of 6 and the comoving emission rate per unit volume of ionizing photons is constant or only very slightly declining at these redshifts. If extrapolated, is still sufficient to maintain a highly ionized IGM to  $z = 6.6$ .

This leaves the longest redshift ( $z = 6.05$ ) point in SDSS 1030+0524 as the single strong piece of evidence for the epoch of reionization lying at  $z = 6.1$ . Cen & McDonald (2001) have used a  $\Lambda$ -dominated cold dark matter (LCDM) model (which provides a good fit to our present data) to analyze the Ly $\alpha$  and Ly $\beta$  absorption of this point, concluding that the  $2\sigma$  upper limit on the ionization rate at this redshift is about half of that which we would deduce from an extrapolation of our lower redshift data. An abrupt drop would be consistent with the Becker et al. and Fan et al. interpretations.

<sup>1</sup>Visiting astronomer, W. M. Keck Observatory, jointly operated by the California Institute of Technology and the University of California.

However, as we show, the lower redshift data is also consistent with models in which there is substantial dispersion in the ionization parameter, or equivalently the equation of state of the gas, and these models have a significant probability of including dark points like that of Becker et al. even for a smooth extrpolution of the mean ionization rate. A conclusive determination of the reionization epoch therefore requires a much larger sample of data at the highest redshifts.

## 2. BACKGROUND

As was first pointed out by Shklovskij (1964), Scheuer (1965) and Gunn & Peterson (1965), a fully neutral intergalactic medium produces an enormous Lyman  $\alpha$  scattering

$$\tau_{\text{H I}} = 3.4 \times 10^5 h^{-1} \left( \frac{\Omega_m}{0.35} \right)^{-0.5} \left( \frac{\Omega_b h^2}{0.0325} \right) \left( \frac{1+z}{7} \right)^{1.5} \quad (1)$$

where, at high redshifts in the currently favored cosmology, the local Hubble constant  $H \approx \Omega_m^{1/2} (1+z)^{3/2} H_0$  (e.g. Barkana 2001). Here  $h = H_0/(100 \text{ km s}^{-1} \text{ Mpc}^{-1})$ ,  $\Omega_m$  is the local mass density and  $\Omega_b$  is the baryon density. Even when the effects of structure are allowed for at these redshifts, the minimum density 'void' regions with baryon densities  $\Delta \equiv \rho_b/\langle \rho_b \rangle \sim 0.1$  would have optical depths in excess of  $10^4$ . A predominantly neutral IGM would therefore produce a totally black Ly $\alpha$  forest region. This is quite unlike the situation seen in the spectra of quasars to  $z = 6.2$  where, as we discuss in detail below, there are still substantial portions of the spectrum in which there is transmitted flux.

In actuality the lower density regions of the IGM will become ionized prior to the point at which the ionized regions merge and the bulk of the mass of the the IGM begins to ionize, which we would consider to be the redshift of reionization (see Miralda-Escudé, Haehnelt & Rees 2000 for a detailed description). The transmission through the underdense ionized regions results in some observable flux. However, even in this limit the radiation damping wings of the neutral hydrogen regions can completely black out the region. A spectrum with portions that are still transmitting in the Lyman  $\alpha$  forest region can correspond to a period near reionization only if the dark gaps produced by the substantial amounts of neutral hydrogen in the high overdensity regions are sufficiently separated. This in turn means that the dark gaps must contain high column densities of neutral hydrogen and be very wide (cf. Barkana 2001).

A simple toy model serves to illustrate this point. Suppose the baryons are substantially neutral (fraction  $f_N$ ) by mass and that all the neutral material is concentrated in a 'picket fence' with the separation between the regions corresponding to a redshift interval  $\Delta z$  or rest-frame wavelength separation  $\Delta \lambda = \lambda_\alpha \Delta z/(1+z)$ . This model neglects the neutral hydrogen opacity contributions from the ionized regions, and so minimizes the 'darkness' of the spectrum. The column density of each spike in the picket fence is now

$$N(\text{H I}) = \left( \frac{c\rho_c}{H_0 m} \right) \Omega_m^{-0.5} (1+z)^{1.5} f_N \Omega_b \frac{\Delta \lambda}{\lambda_\alpha} \quad (2)$$

where  $\rho_c$  is the closure density,  $m$  the mass per hydrogen atom and  $\lambda_\alpha$  is the Lyman  $\alpha$  wavelength. Neutral hydrogen regions have a damped Lyman  $\alpha$  equivalent width of

$$W_\alpha = 23.2 \left( \frac{N(\text{H I})}{10^{21} \text{ cm}^{-2}} \right)^{0.5} \text{ \AA} \equiv 23.2 N_{21}^{0.5} \text{ \AA} \quad (3)$$

and produce dark regions

$$\Delta \lambda_{2.5} = 8.3 N_{21}^{0.5} \text{ \AA} \quad \text{and} \quad \Delta \lambda_{1.25} = 11.7 N_{21}^{0.5} \text{ \AA} \quad (4)$$

where  $\Delta \lambda_{2.5}$  is the width of the region with  $\tau > 2.5$  and  $\Delta \lambda_{1.25}$  is that at  $\tau = 1.25$ . In order to produce regions with  $\tau < 2.5$  in the spectra,  $\Delta \lambda > \Delta \lambda_{1.25}$ , which requires

$$N_{21}^{0.5} > 1.2 f_N \left( \frac{\Omega_m}{0.35} \right)^{-0.5} \left( \frac{\Omega_b h^2}{0.0325} \right) \left( \frac{h}{0.65} \right)^{-1} \left( \frac{1+z}{7} \right)^{1.5} \quad (5)$$

or minimum gap lengths at  $\tau = 2.5$  of

$$\Delta \lambda_{2.5} > 10 \text{ \AA} f_N \left( \frac{\Omega_m}{0.35} \right)^{-0.5} \left( \frac{\Omega_b h^2}{0.0325} \right) \left( \frac{h}{0.65} \right)^{-1} \left( \frac{1+z}{7} \right)^{1.5}. \quad (6)$$

This is an extreme lower limit: complexifying the neutral hydrogen structure or including the opacity effect of the ionized gas will only raise  $\Delta \lambda_{2.5}$ . In essence, we must concentrate the neutral hydrogen to produce transmission gaps, and these concentrations will in turn produce very wide dark regions. Thus, a key signature of the approach to reionization is the onset of either a *completely black* spectrum or of many *wide* dark regions.

However, distinguishing this from a highly ionized post-reionization intergalactic medium may be extremely difficult. At these redshifts, a uniform ionized IGM would have a Ly $\alpha$  optical depth

$$\tau_u = 14 \Gamma_{-12}^{-1} T_4^{-0.75} \left( \frac{\Omega_m}{0.35} \right)^{-0.5} \left( \frac{\Omega_b h^2}{0.0325} \right)^2 \left( \frac{H_0}{65 \text{ km s}^{-1} \text{ Mpc}^{-1}} \right)^{-1} \left( \frac{1+z}{7} \right)^{4.5} \quad (7)$$

where  $\Gamma_{-12}$  is the local ionization rate produced by the metagalactic ionizing flux in units of  $10^{-12} \text{ s}^{-1}$  and  $T_4$  is the gas temperature in units of  $10^4 \text{ K}$ . The corresponding optical depth at Ly $\beta$  is a combination of the direct Ly $\beta$  absorption and Ly $\alpha$  absorption at the redshift

$$1 + z_\beta \equiv \left( \frac{\lambda_\beta}{\lambda_\alpha} \right) (1 + z) \quad (8)$$

where  $\lambda_\alpha$  and  $\lambda_\beta$  are the Ly $\alpha$  and Ly $\beta$  wavelengths, and is given by

$$\tau_{\beta_u} = 0.16 \tau_u(z) + \tau_u(z_\beta) \quad (9)$$

The two terms in equation (9) are generally comparable, the exact ratio being dependent on the steepness of the evolution of  $\tau_u$  with  $(1+z)$ . Thus, even in this limit, transmission again will be seen only in the most underdense 'void' regions of the IGM, with most of the spectrum again being black even at Ly $\beta$ . (Because of the very steep redshift dependence, this is unlike the situation at lower redshifts,  $z \sim 3$ , where even the mean density regions have significant Ly $\alpha$  transmission.)

The distribution of the transmission and the mean transmitted flux depend in this high redshift limit on the fraction of the volume occupied by regions of low density (which in turn primarily depends on the details of the cosmological model) and on the normalized ionization rate

$$g \equiv \Gamma_{-12} T_4^{0.75} \left( \frac{\Omega_m}{0.35} \right)^{0.5} \left( \frac{\Omega_b h^2}{0.0325} \right)^{-2} \left( \frac{H_0}{65 \text{ km s}^{-1} \text{ Mpc}^{-1}} \right) \quad (10)$$

which specifies the neutral fraction at  $\Delta = 1$  (see McDonald & Miralda-Escudé 2001). For a specified cosmological model, the mean transmitted flux in the spectrum can be used to obtain  $g$  and so the evolution of the ionizing flux with redshift (McDonald & Miralda-Escudé 2001; Cen & McDonald 2001). If we ignore the effects of thermal broadening and peculiar motions, and also assume that the gas has an equation of state  $T \sim \Delta^{\gamma-1}$ , we can generalise equation (7) to obtain the optical depth of the fluctuating medium

$$\tau_\Delta = 14 g^{-1} \left( \frac{1+z}{7} \right)^{4.5} \Delta^\beta \quad (11)$$

where  $\beta = 2 - 0.75(\gamma - 1)$  and  $\tau_\Delta$  is the optical depth at a point in the spectrum corresponding to a spatial position with normalized density  $\Delta$  (e.g. Hui & Gnedin 1997). It can be seen immediately from equation (10) that transmission regions with  $\tau < 1$  will correspond to normalized densities of less than or around  $\Delta = 0.27 g^{-0.5}$  at  $z = 6$ , where for simplicity we have assumed an isothermal equation of state. Because the volume occupied by low density regions drops rapidly with decreasing  $\Delta$ , the mean transmission comes from a sharply peaked region of  $\Delta$ . If we adopt (as did Fan et al. 2001b) the form of the volume density distribution function given by Miralda-Escudé, Haehnelt & Rees (2000)

$$P(\Delta) d\Delta = A \Delta^{-b} \exp \left( \frac{-(\Delta^{-2/3} - C)^2}{8\delta_0^2/9} \right) d\Delta \quad (12)$$

where  $b \approx 2.5$  at high redshift and  $A$  and  $C$  are specified by the normalization of  $P$  and the condition  $\bar{\Delta} = 1$ , then ignoring the normalizing constant  $C$  term in the low density regime, the mean transmitted flux has the form

$$F = \int A \Delta^{-b} \exp - \left( \tau_u \Delta^\beta + \frac{\Delta^{-4/3}}{8\delta_0^2/9} \right) d\Delta \quad (13)$$

The exponent peaks sharply at

$$\Delta_0 = \left( \frac{3}{2\tau_u \beta \delta_0^2} \right)^{\frac{1}{\beta+4/3}} \quad (14)$$

which, adopting  $\delta_0 = 7.61(1+z)^{-1}$  appropriate to the LCDM model of Miralda-Escudé et al. (1996), corresponds to

$$\Delta_0 = 0.39 g^{0.3} \left( \frac{1+z}{7} \right)^{-0.75} \quad (15)$$

and where we have again used the isothermal equation of state for simplicity. We can now evaluate the integral using the

method of steepest descents to give

$$F(z, g) = A \left( \frac{4\pi}{3\beta + 4} \right)^{0.5} \delta_0 \Delta_0^{5/3-b} \exp \left( - \left( \frac{3}{2\beta} + \frac{9}{8} \right) \Delta_0^{-4/3} \delta_0^{-2} \right) \quad (16)$$

where, for the isothermal  $\beta = 2$ , the exponent becomes  $-5.56g^{-0.4}((1+z)/7)^3$ , so that the effect of the structure is to make the evolution of the effective optical depth  $-\ln T$  with redshift shallower than in the uniform case (e.g. Bi & Davidsen 1996). The dependence on the equation of state is extremely weak. Inclusion of the  $C$  term changes the integral slightly, but adopting this functional form, we use the analytic equation

$$F(z, g) = 4.5 g^{-0.28} \left( \frac{1+z}{7} \right)^{2.2} \exp \left( -4.4 g^{-0.4} \left( \frac{1+z}{7} \right)^3 \right) \quad (17)$$

which provides an accurate representation (a maximum of 8% deviation from  $g = 0.2$  to  $g = 3$ ) of the LCDM numerical models of McDonald & Miralda-Escudé (2001), Cen & McDonald (2001) and Cen & McDonald (2002, in preparation) and to the exact integral obtained using equations (11) and (12) over the  $z = 4 - 6$  redshift range of interest.

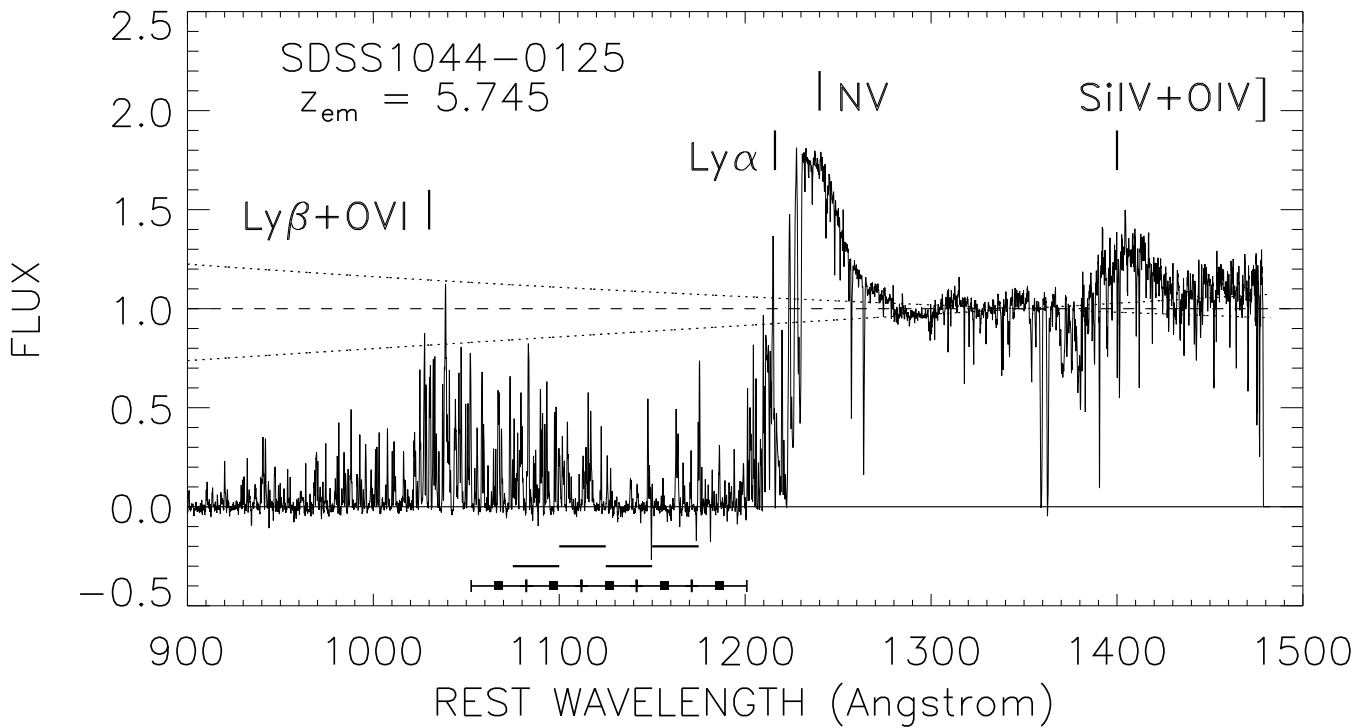


FIG. 1.— Spectrum of the quasar SDSS1044–0125 taken with ESI on KeckII (see Table 1). The emission redshift of 5.745 was adopted from Goodrich et al. (2001) and the positions of emission lines of Ly $\beta$ +O VI, Ly $\alpha$ , N V and Si IV+O IV] are shown as short vertical lines. The spectrum is shown smoothed to 0.25 Å and normalized in the region of 1330 – 1370 Å in the rest frame to a power-law continuum ( $f_\lambda$ ) with slope  $-1.25$  (solid line). The dotted lines show continua with slopes  $-0.75$  and  $-2$ . The short horizontal lines below the spectrum show the positions of the wavelength bins used to calculate the transmitted fluxes in Figures 5 and 6; they are 1075 – 1100 Å, 1100 – 1125 Å, 1125 – 1150 Å and 1150 – 1175 Å in the rest frame. The bins used by Becker et al. (2001) are shown below that by the horizontal lines with the centers shown by small filled squares. Associated absorption can be seen in the Si IV line at wavelengths shortward of the Si IV emission. Based on the corresponding C IV, Goodrich et al. (2001) described this as a BAL QSO.

### 3. OBSERVATIONS

A total of 15 high redshift quasars, with  $4.42 < z_{\text{em}} < 5.745$ , were observed for this program (Table 1) using the Echellette Spectrograph and Imager (ESI; Sheinis et al. 2000) instrument on the KeckII telescope in echellette mode. The

resolution in this configuration is comparatively low,  $\sim 5300$  for the  $0.75''$  slit width used, but the red sensitivity of the instrument is high and the wavelength coverage is complete from  $4000 \text{ \AA}$  to  $10,000 \text{ \AA}$ . At the red wavelengths, extremely high precision sky subtraction is required since the sky lines can be more than two orders of magnitude brighter than the quasars. In order to deal with this issue, individual half-hour exposures were made, stepped along the slit, and the median was used to provide the primary sky subtraction. Total exposure times are given in Table 1. The frames were then registered, filtered to remove cosmic rays and artifacts, and then added. At this point a second linear fit to the slit profile in the vicinity of the quasar was used to remove any small residual sky. The observations were made at the parallactic angle and flux calibrated using observations of white dwarf standards scattered through the night. These standards were also used to remove telluric absorption features in the spectra, including the various atmospheric bands. The final extractions of the spectra were made using a weighting provided by the profile of the white dwarf standards. Wavelength calibrations were obtained using third-order fits to CuAr and Xe lamp observations at the beginning and end of each night, and the absolute wavelength scale was then obtained by registering these wavelength solutions to the night sky lines. The wavelengths and redshifts are given in the vacuum heliocentric frame.

The quality of the data and the extraction is shown in Figure 1 for the highest redshift QSO in the sample, SDSS 1044–0125, which also has one of the lowest S/N in the sample. The total exposure time was 5.75 hours. The spectrum is shown smoothed to  $0.25 \text{ \AA}$  and normalized in the region of  $1330 - 1370 \text{ \AA}$  in the rest frame to a power-law continuum ( $f_\lambda$ ) with slope  $-1.25$  (solid line). The dotted lines show continua with slopes  $-0.75$  and  $-2$ . For this range of slopes there is a  $\pm 18 \%$  range in the normalization at  $1075 \text{ \AA}$ . We adopt the emission redshift of  $5.745$  for this quasar, which Goodrich et al. (2001) measured from NIRSPEC spectroscopy of the C IV emission line and associated absorption that they describe as BAL-like. This associated absorption is only very weakly seen in the blue wing of the Si IV line and the Si IV + O IV] emission gives a consistent solution for the emission redshift. The short vertical bars above the spectrum show the resulting positions of the Ly $\beta$ +O VI, Ly $\alpha$ , N V and Si IV + O IV] emission lines.

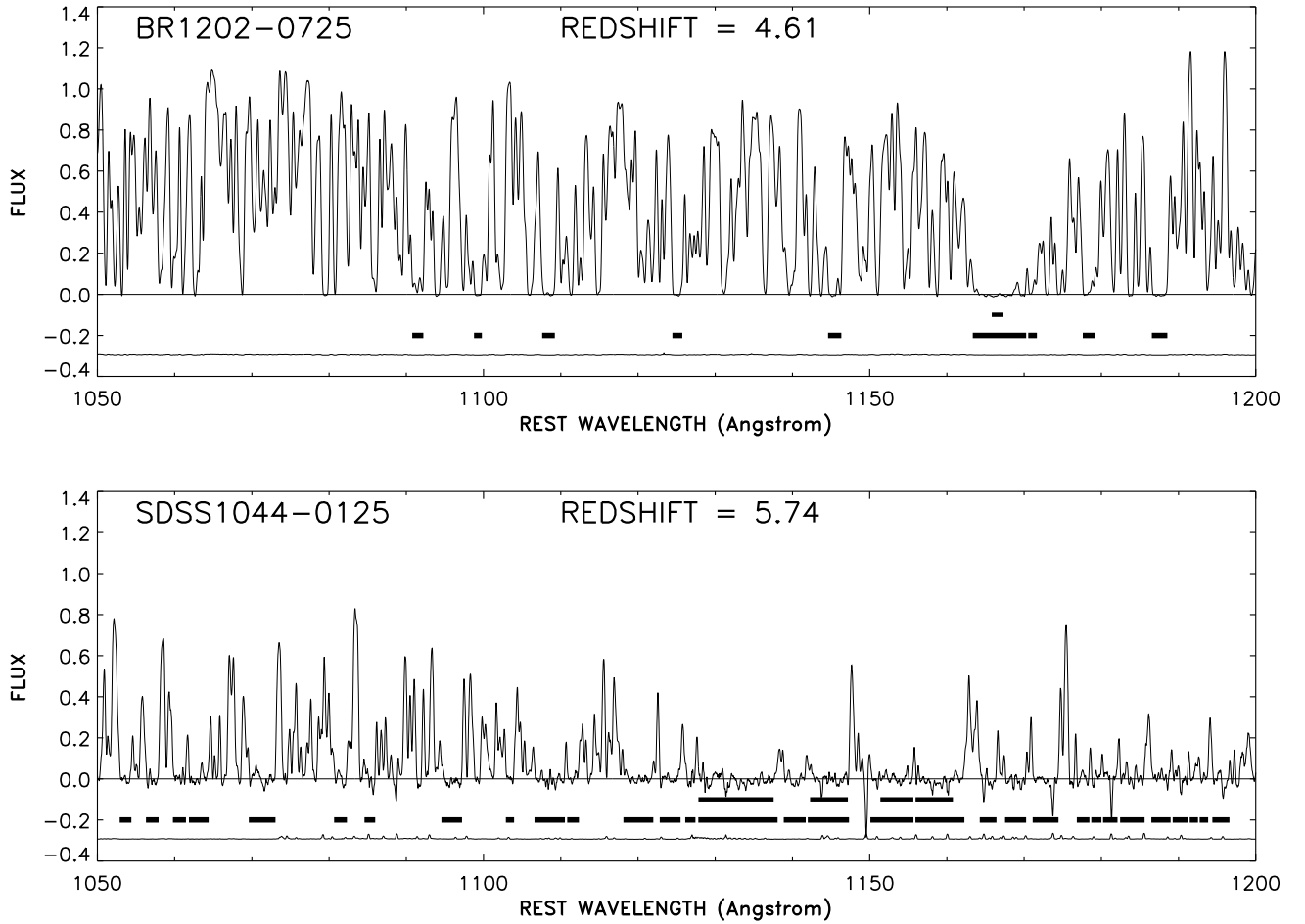


FIG. 2.— Portions of the spectra between rest wavelengths of  $1050 \text{ \AA}$  and  $1200 \text{ \AA}$  for (top panel) BRI 1202–0725 ( $z_{em} = 4.61$ ) and (bottom panel) SDSS 1044–0125 ( $z_{em} = 5.74$ ), normalised to a power law continuum with slope  $-1.25$ . The formal statistical noise is shown in a panel below each spectrum. The black bars plotted immediately above the noise show regions in the spectrum that have Ly $\alpha$  optical depth,  $\tau_{Ly\alpha} > 2.5$  over a rest-frame width  $> 1 \text{ \AA}$ . On the line above, similar black bars mark regions of the spectra where the optical depth and width criteria also hold at the position of Ly $\beta$  in each spectrum.

The region of primary interest between 1050 Å and 1200 Å is shown in more detail in Figure 2 for SDSS 1044–0125 and for the lower redshift and the more typical S/N spectrum of BRI 1202–0725, both of which contain wide saturated regions which can be used to estimate the accuracy of the sky subtraction. The formal statistical noise derived for the spectra is shown underneath the spectrum in each panel. In general, however, systematic residuals associated with strong night sky lines are a larger source of noise, as can be clearly seen in SDSS 1044–0125. In the base of the damped Ly $\alpha$  line at  $z = 4.383$  in BRI 1202–0725 we measure a mean normalized flux of  $-0.002$  while in the dark region at  $z = 5.286$  in SDSS 1044–0125 we measure  $-0.009$ , suggesting that the sky subtraction leaves about 1% residuals in the faintest quasars and smaller errors in the brightest ones. We take the larger value as our systematic error.

#### 4. TRANSMITTED FLUXES AND THE EVOLUTION OF THE IONIZING PARAMETER

The simplest quantity that can be used to characterize the Lyman alpha forest is the mean reduction which it introduces in the continuum. Oke & Korycansky (1982) introduced the  $D_A$  index, defined as

$$D_A = \left\langle 1 - \frac{F_\nu}{F_{\nu 0}} \right\rangle \quad (18)$$

where  $F_\nu$  is the actual flux and  $F_{\nu 0}$  is the continuum, and the average is over rest-frame wavelengths from 1050 Å to 1170 Å, which makes this measurement over most of the Ly $\alpha$  forest region. We show this quantity in Figure 3 where, to make the most direct comparison with the lower redshift points of Schneider, Schmidt & Gunn (1991) and Kennefick, Djorgovski & de Carvalho (1995), we used a spectral index of 0.9 in extrapolating the continuum, equal to the mean Schneider et al. value. (The choice of continuum can shift the points vertically by offsets of up to 0.2). We have also shown the values measured by Becker et al. (2001) in the three of their four quasars that do not overlap with the present sample. The present data show a smooth connection between the high and low redshifts, indicating the rapid drop in the transmitted flux as we move to the higher redshifts.

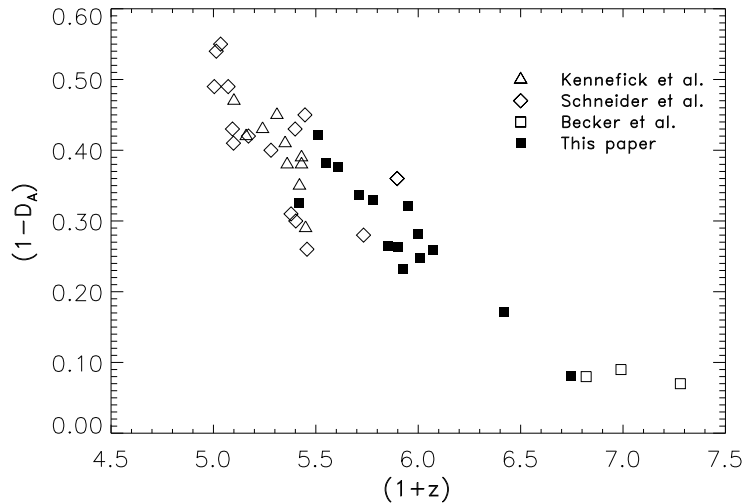


FIG. 3.— Plot of  $1 - D_A$ , the Oke index, for the data of this paper (filled squares), Becker et al. (2001; open squares), Kennefick, Djorgovski & de Carvalho (1995; open triangles) and Schneider, Schmidt & Gunn (1991; open diamonds).

The quality of the present spectra justifies a more detailed analysis, and for each quasar transmitted fluxes blueward of the Ly $\alpha$  emission were then measured in four bins with rest wavelengths of 1150–1175 Å, 1125–1150 Å, 1100–1125 Å and 1075–1100 Å. For SDSS 1044–0125, these bins are illustrated as short horizontal bars below the spectrum in Figure 1. For the remainder of the paper we use the  $-1.25$  power law continuum from Figure 1. The contiguous wavelength bins used by Becker et al. (2001) in calculating transmitted fluxes for this quasar are also shown in Figure 1 with centers marked by the small squares. It can be seen that the Becker et al. bins extend considerably closer to the quasars' Ly $\alpha$  and Ly $\beta$  emission, where the emission line flux might affect the normalization, which is why we adopt the present intervals. Measurements made closer to the quasar redshift might also be more vulnerable to effects associated with the quasar itself, as we discuss further below. Some idea of the possible errors in the transmitted fluxes in the shorter exposure Becker et al. data can be gained from Figure 4, which is a comparison of the transmitted fluxes in 1044–0125 given by Becker et al. with the fluxes measured in the Becker et al. bins in the spectrum of Figure 1. At these low fluxes, the statistical errors in the present spectra are tiny, and even the systematic errors from continuum fitting (see Figure 5 caption) are very small. Despite this, there are clearly substantial differences between the Becker et al. points and the present data, which are most probably related to the sky subtraction issue and to the lower S/N of the Becker et al. data. The two highest wavelength points are a factor of 1.7 lower than the Becker et al. numbers.

The mean transmitted flux in these bins versus redshift is shown in Figure 5 for the entire sample (filled squares). The  $1 \sigma$  statistical error together with the continuum fitting uncertainty is shown as a vertical error bar which is, however,

sometimes smaller than the plotting symbol, and the width of the bin is shown by the horizontal line. The continuum fitting errors strongly dominate, particularly at higher transmission. We also show (open squares) the transmitted fluxes measured by Becker et al. in their three quasars that do not overlap with the present sample. The overall sample shows a smooth decline with redshift, albeit with a substantial scatter. A least squares fit to a power law of the form  $F \propto (1+z)^x$  gives  $x = -7.1$  if we use only the present data (solid line in Figure 5) and  $-8.1$  if we include the Becker et al. data (dashed line).

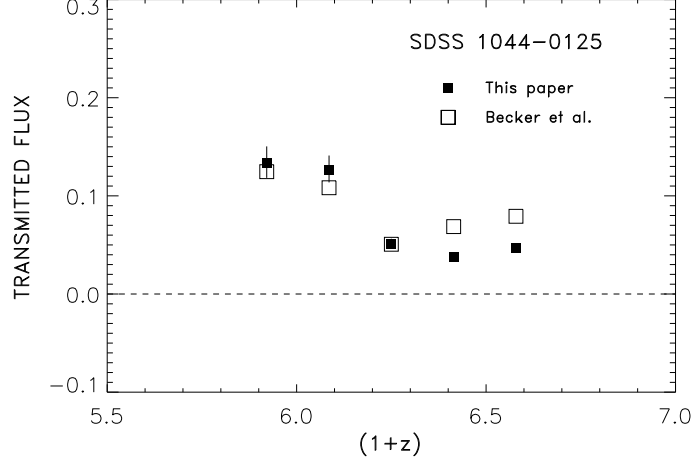


FIG. 4.— Comparison of the transmitted flux blueward of  $\text{Ly}\alpha$  in the quasar SDSS1044–0125 determined by this paper (filled squares) and by Becker et al. (2001; open squares). The error bars are described in Figure 5.

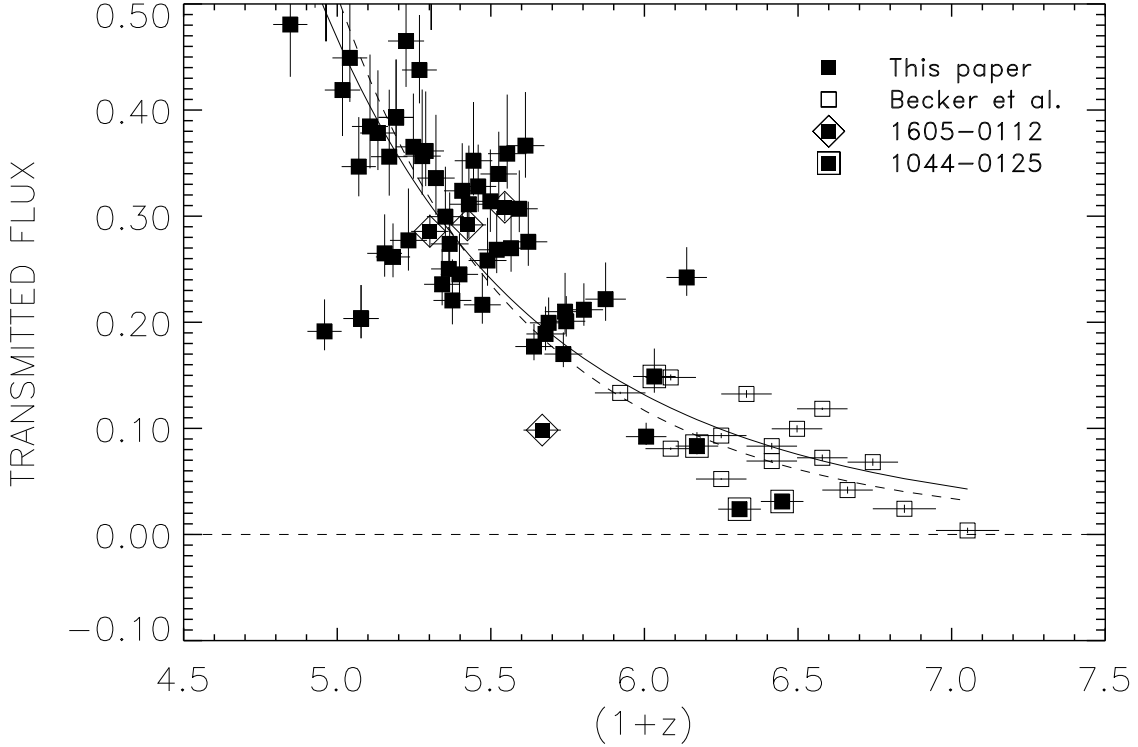


FIG. 5.— Plot of transmitted flux vs  $(1+z)$  for the data of this sample (filled squares) and of Becker et al. (1001; open squares). (Statistical) error bars from Becker et al. are shown as vertical lines. For the present sample, the error bars are a combination of statistical errors and errors from varying the continuum fit (see Figure 1); in some cases they are smaller than the data boxes. These errors are strongly dominated by the continuum fitting error. The transmitted fluxes of the possible BAL QSO SDSS1044–0125 and of the BAL QSO SDSS1605–0122 are marked. (The latter object is excluded from the sample.) The solid and dashed lines are fits of the form  $F \propto (1+z)^x$ . The solid line is fitted only to the present data, and has an index of  $-7.1$  whereas the dashed line fit includes the Becker et al. data and has an index of  $-8.1$ .

At a given redshift, the scatter in the transmitted flux represents the variance produced by different sampling of the density distribution function (and possibly the variation in the ionization parameter  $g$ ) in the wavelength average over the particular bin. However, some part of this scatter appears to be associated with intrinsic quasar absorption. Two of the quasars, SDSS 1605–0112 and SDSS 1044–0125, show BALQSO behaviour. SDSS 1605–0112 is a clear BALQSO and SDSS 1044–0125 has strong associated lines that were described by Goodrich et al. (2001) and can also be seen in Figure 1 in Si IV. We have distinguished the transmitted flux from these quasars in Figure 5, and in both cases, the longest wavelength points appear anomalously low compared with the typical value. It appears probable that this is being caused by Ly $\alpha$  opacity associated with the quasar. This type of behaviour is clearly not uncommon, with 2 of the current sample of 15 quasars falling into that category. We do not yet know whether the highest redshift quasars in the Becker et al. sample are of like type, which could result in low transmission in the highest redshift point, and this is clearly an issue that must be checked (but see Pentericci et al. 2001). We have (slightly arbitrarily) excluded SDSS 1605–0112 but not SDSS 1044–0125, from the sample at this point, but the results are not significantly affected by the inclusion or exclusion of either object.

We next formed the mean transmitted flux averaged over the measured values from the full sample of quasars in the given redshift bin (including the data of Becker et al. (2001) for the three non-overlapping quasars) and also the variance in the points, which we used to determine the uncertainty in the mean. The mean values and errors are summarized in Table 2 and shown as the large filled diamonds in Figure 6, where we have plotted the mean optical depth,  $\bar{\tau}$ , defined as  $-\ln(\text{mean transmitted flux})$ , versus  $\ln(1+z)$  so that the power law fits, which are again illustrated, appear as straight lines. We have also shown the individual data points. The evolution of the mean optical depth from  $z = 4$  to  $z = 6$  is well represented by

$$\bar{\tau} = 3.5 + 8.1 \ln \left( \frac{1+z}{7} \right) \quad (19)$$

which corresponds to a mean transmission relation of

$$F = 0.031 \left( \frac{1+z}{7} \right)^{-8.1} \quad (20)$$

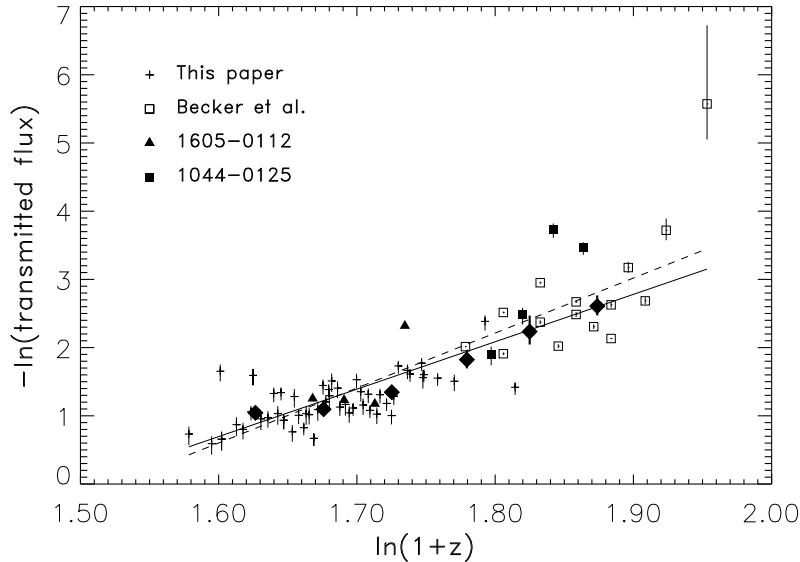


FIG. 6.— Plot of  $-\ln(\text{transmitted flux})$  vs  $\ln(1+z)$  for the data of this sample (crosses) and of Becker et al. (2001; open squares). Error bars as described in Figure 5 are shown only for the Becker et al. points. Filled squares show the values for the BAL QSO SDSS 1044–0125, and filled triangles for the BAL QSO SDSS 1605–0122 (which is not included in the sample). The solid line is a power law of slope 7.1 fitted to the data of the current sample, excluding the Becker et al. (2001) data, but including SDSS 1044–0125. The dashed line is a power law of slope 8.1 fitted to all the data except SDSS 1605–0122. Filled diamonds show the average of all the data except SDSS 1605–0122 in bins of width 0.05 in the log for  $1.6 < \ln(1+z) < 1.9$ , with error bars showing the  $\pm 1 \sigma$  error in the mean.



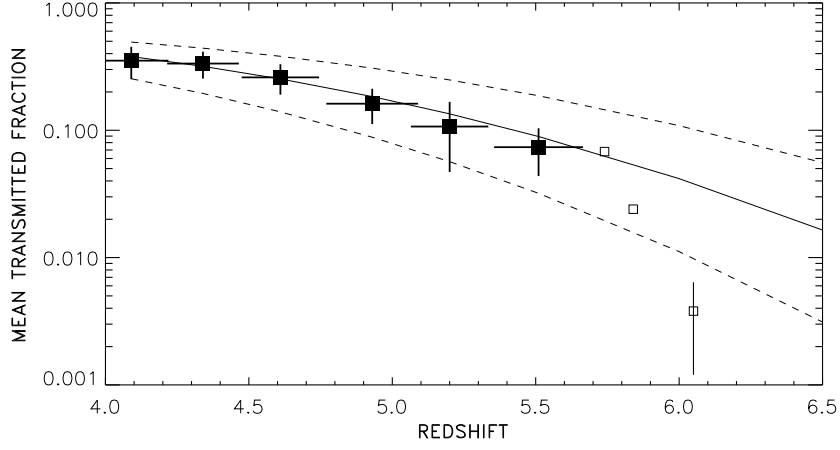


FIG. 7.— The mean transmitted flux as a function of redshift (filled squares) compared with the expected transmission as a function of the ionization parameter  $g$  (equation 17). The model is shown for  $g = 0.86$  (solid line) and  $g = 0.43$  and  $g = 1.72$  (dashed lines). The error bars show the variance in the individual measurements (rather than the error in the mean) to illustrate the uncertainty (roughly a factor of 2) that would be associated with measuring only a small number of transmissions at a given redshift. Above  $z = 5.7$  we show the individual data points of Becker et al. (2001) as small open squares. For these Becker et al. points, the error bar is the statistical uncertainty associated with the individual point.

We can now use equation(17) to translate the mean transmissions to ionization rates. The mean transmission and the variance of the transmission are compared in Figure 7 with the expected evolution with  $z$  for an ionization parameter  $g = 0.86$  which produces rough agreement with the data points over the redshift range (solid line). We also show the transmissions expected when  $g$  is changed by a multiplicative factor of 2 in either direction, which roughly corresponds to the variance, and provides a measure of how much uncertainty would be expected from measuring  $g$  from a small number of quasars. This can be used to assess the uncertainties in the measurements from the individual Becker et al. (2001) data points at the highest redshifts.

In Figure 8 we show the direct inversion to obtain  $g$  in each redshift bin (filled points). Here the error bars correspond to the error in the mean transmission. We have also shown  $g$  determined by McDonald et al. (2000) at lower redshift (open squares) and the values that would be determined from the three individual Ly $\alpha$  points in the Becker et al (2001) data at longer redshift (small open diamonds). As was shown in Figure 7, the present data points are consistent with being constant as a function of redshift but the combination with the lower redshift data points shows that the ionization parameter can be quite well represented by a power law of the form

$$g = 41 (1 + z)^{-2.2} \quad (21)$$

which is shown as the solid line in Figure 8. Only the  $z = 4$  data point deviates substantially from this form and this is the most uncertain point because of the continuum extrapolation. In contrast to the results of Cen & McDonald (2001), whose findings were based on a small data sample, we find no significant structure or peaks in the ionization function that might be associated with the period just following reionization. Instead, with the single exception of the highest redshift Becker et al. (2001) point, all the data are consistent with a smooth evolution to  $z = 6$ . The possibility that the reionization epoch is at  $z \sim 6.1$  stands or falls, therefore, on this single data point at  $z = 6.05$ .

$g$  is related to the comoving production rate of ionizing photons,  $\dot{n}_I$ , released to the IGM by the relation

$$\dot{n}_I (1 + z)^3 = \frac{\Gamma}{\sigma \Delta \lambda} \quad (22)$$

(e.g. McDonald & Miralda-Escudé 2001) where  $\Delta \lambda$  is the proper distance between absorbers and  $\sigma$  is the mean cross section for ionization. Madau, Haardt & Rees (1999) give  $\Delta \lambda = 33 \text{ Mpc}(1 + z)^{-4.5}$  and using this form, setting  $\sigma = 2 \times 10^{-18} \text{ cm}^{-2}$ , and adopting the cosmology of section 2 so that  $\Gamma = 10^{-12} g \text{ s}^{-1}$ , we have

$$\dot{n}_I \approx 2 \times 10^{-19} (1 + z)^{-0.7} \text{ cm}^{-3} \text{ s}^{-1} \quad (23)$$

so that the comoving production rate of ionizing photons is varying only slowly with redshift. We can integrate equation (23) to find the total comoving number density of ionizing photons produced at redshift  $z$ ,

$$n_I(\text{tot}) = 0.5 H_0^{-1} \Omega_m^{-0.5} (1 + z)^{-1.5} \dot{n}_I \approx 5 \times 10^{-2} (1 + z)^{-2.2} \text{ cm}^{-3} \quad (24)$$

which is more than sufficient to ionize the hydrogen density ( $n_{H_0} = 2.6 \times 10^{-7} \text{ cm}^{-3}$  with the presently adopted parameters) out to the highest observable redshifts, even allowing for the multiplicative factor of several uncertainty in the ratio of  $n_I(\text{tot})$  to  $n_{H_0}$  which is present in (21) from the adopted cosmology and the equation of state.

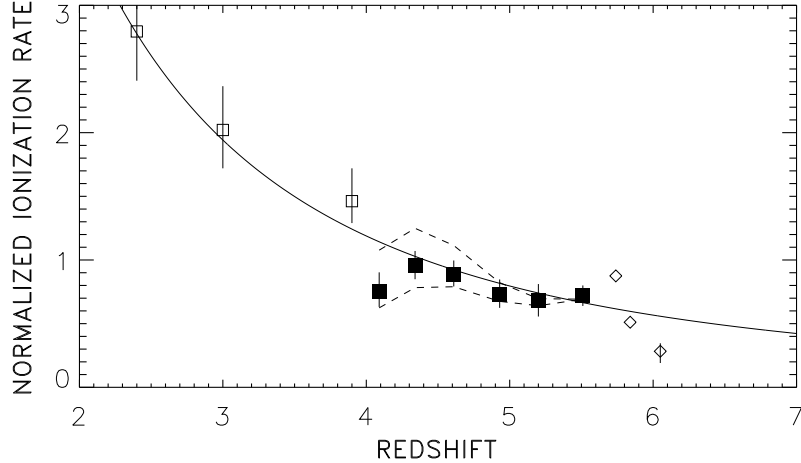


FIG. 8.— The evolution of the ionization parameter  $g$  as a function of redshift computed from the mean transmissions using equation 15 (filled squares). The error bars correspond to errors in the mean. The open squares show the measurements of McDonald et al. at lower redshifts. The small open diamonds show the values measured from the individual Becker et al. (2001) data points at higher redshift. The solid line shows a fit of the form  $g = 41(1+z)^{-2.2}$  which provides a reasonable description of the evolution of the ionization parameter from  $z = 2$  to  $z = 6$ . The dashed lines show the systematic errors which could be produced by the choice of the continuum fit.

##### 5. THE DISTRIBUTION OF TRANSMISSIONS AND THE INCIDENCE OF DARK GAPS

At redshifts  $z > 5$  it is no longer possible to carry out the kind of Voigt profile analysis of the spectrum that has been used extensively at lower redshifts (e.g. Hu et al. 1995; Kirkman & Tytler 1997; Kim et al. 1997). However, subject to the uncertainties in the continuum extrapolation used to normalize the spectrum (primarily important at low optical depths), we can measure alternative quantities to characterise the spectra and compare with models, such as the distribution of the transmissions (e.g. Rauch et al. 1997) or the frequency of gaps (e.g. Croft 1998).

The simplest quantity that can be used to quantify the spectra is the cumulative distribution of transmissions, which primarily depends only on the distribution of the neutral hydrogen density at a particular redshift and contains little information about the velocity structure. We have computed this quantity from the present observations for three redshift intervals [4.25,4.75], [4.95,5.45] and [5.45,5.95]. The first two redshift intervals are chosen to match the LCDM models presented by McDonald & Miralda-Escudé (2001). The observational results are shown as the crosses in Figure 9, where low redshift is at the bottom of the figure and the highest redshift is at the top. We also show the model distributions at  $z = 4.5$  (squares) and  $z = 5.2$  (diamonds) from the LCDM numerical calculations, with ionization parameters chosen to match the observations. (The ionization rates are in reasonable agreement with the values computed in the previous section from the mean transmissions.) This model agrees very well with the data, as was also found by Fan et al. (2001b). We can approximate the numerical models by combining equations (11) and (12) and this result is shown as the solid lines in Figure 9. We have used this to extend the comparison of the model to  $z = 5.7$  where it remains in good agreement with the observations.

Cen & McDonald used this LCDM model to assess the probability of seeing a dark transmission region similar to that in the highest redshift Becker et al. (2001) point. Using the more stringent constraint from  $\text{Ly}\beta$ , they found that there was a  $2\sigma$  probability of seeing such a feature if their  $\Gamma_{-12}$  obeyed the relation  $\Gamma_{-12} \leq 0.062$ , which corresponds to  $g = 0.3$  in the present notation. This can be compared to the value of  $g = 0.6$  expected at  $z = 6.05$  from equation (19) and might suggest the beginning of a substantial drop in  $g$ , consistent with the Becker et al. (2001) interpretation.

However, one possible problem with the models could lie in the assumption of a constant ionization rate and equation of state (subsumed here in the quantity  $g$ ) at a given redshift. Spatially correlated variations in these quantities could be present even at post-reionization epochs and could substantially change the probability of seeing dark gaps. Clearly, if the distribution of the  $g$  parameter were too broad, it would significantly change the shape of the transmitted fraction shown in Figure 9, but within the uncertainties in the data and the continuum normalization there is considerable latitude for such a possibility. We illustrate this in Figure 10 in which we have again used equations (11) and (12) to construct the cumulative probability of the transmission being below the given value. For redshifts 5.2 and 5.7 we show the data and the cumulative probability with a single ionization parameter  $g$  chosen to optimize the fit. We then show two models, in

one of which half the points in the spectrum have an ionization rate  $0.5g$  (dashed line) and in the other of which half the points have an ionization rate  $0.25g$  (dotted line). In each case we have adjusted the ionization range in the remaining half of the points to optimize the fit. At  $z = 5.2$ , the dotted line is substantially too high at low transmissions and it is clear that a spread in ionization rate of a factor of 4 would produce too many dark regions in the spectra; however, factors of 2 variation are quite acceptable. By  $z = 5.7$ , as the number of dark regions increases, even a factor of 4 variation is not ruled out. If such variations are present then the probability of seeing a dark gap such as that seen by Becker et al. rises substantially, and their result can be understood without invoking reionization (though such variations in the ionization and equation of state, if present, might be related to post-reionization effects).

To proceed further on these lines would require extensive simulations and consideration of the physical processes that might give rise to such variations. An alternative approach is to look at the distribution of dark gaps and the distribution of dark regions in the present data which can, in principle, provide a more sensitive diagnosis of whether there are spatially underionized regions. One simple parameterization is the distribution of the widths of contiguous regions with optical depth greater than or equal to a particular value (Croft 1998). In Figure 2 we show the contiguous regions satisfying the condition  $\tau > 2.5$  over rest-frame wavelength intervals  $> 1 \text{ \AA}$  in the quasar BR 1202–0725 ( $z_{em} = 4.61$ ) and in SDSS 1044–0125 ( $z_{em} = 5.74$ ). As would be expected from the increasing opacities, the frequency of such gaps increases rapidly with redshift. We have also shown the regions where the same condition holds also at  $\text{Ly}\beta$ . Only one region in BR 1202–0725 (the DLA at  $z = 4.383$ ) appears, but even by  $z = 5.3$ , wide systems that are dark in both  $\text{Ly}\alpha$  and  $\text{Ly}\beta$  are becoming common. We illustrate the distribution of the gaps in Figure 11 where we show the number of gaps versus the wavelength per unit redshift interval,  $dX \equiv \Omega_m^{-0.5} (1+z)^{0.5} dz$ . Below  $z = 5$ , the distribution of gaps varies fairly slowly but at  $z > 5$  the number of wide gaps increases rapidly. Again, further analysis requires more detailed simulations.

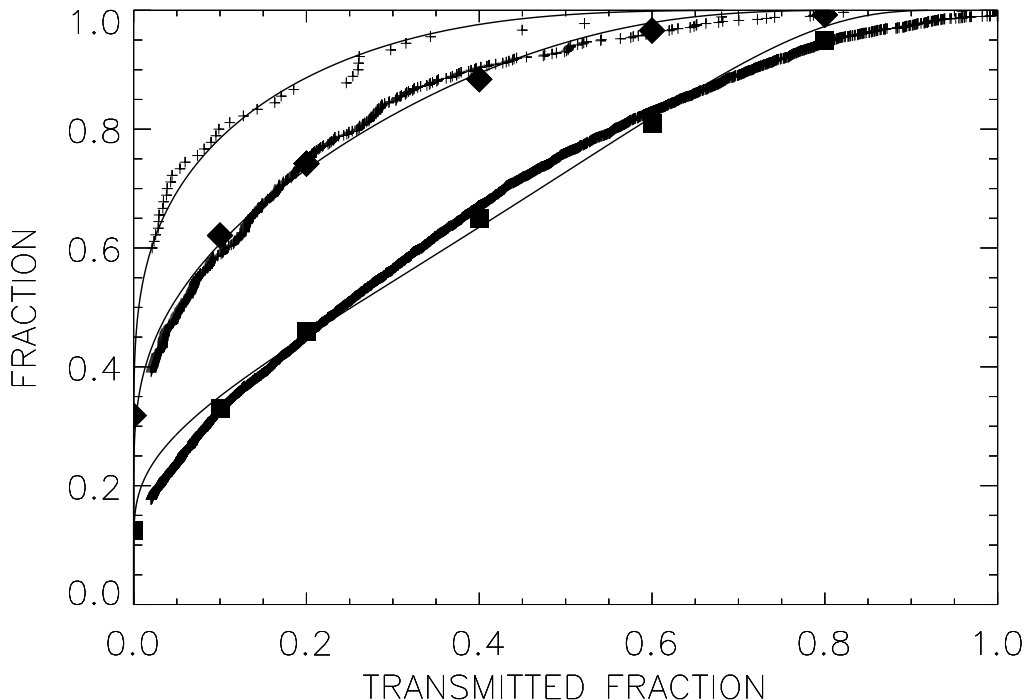


FIG. 9.— The crosses show the cumulative distribution of the transmission fraction for three redshift intervals ( $z = 4.25 - 4.75$ , bottom) ( $z = 4.95 - 5.45$ , middle) and ( $z = 5.45 - 5.95$ , top). The measured values are compared with the results predicted by the LDCM model of McDonald and Miralda-Escudé at  $z = 4.7$  (squares) and  $z = 5.2$  (diamonds) where we have used  $\Gamma_{-12} = 0.28$  at the lower redshift and 0.23 at the higher, in their units, corresponding to  $g = 1.2$  at  $z = 4.5$  and  $g = 0.9$  at  $z = 5.2$ . The model is in excellent agreement with the data. We also show as solid lines the values computed by combining the density distribution function of equation (12) with the opacity relation of equation (11) for an equation of state corresponding to  $\beta = 1.75$ . The analytic approximation provides a reasonable representation of the numerical models and the data at the two lower redshifts, and matches well to the data at  $z = 5.7$  for a choice of  $g = 0.9$ . The exact shape at the high transmission end is sensitive to the extrapolated continuum. This error corresponds to a multiplicative rescaling of the x-axis by a factor of up to 1.2.

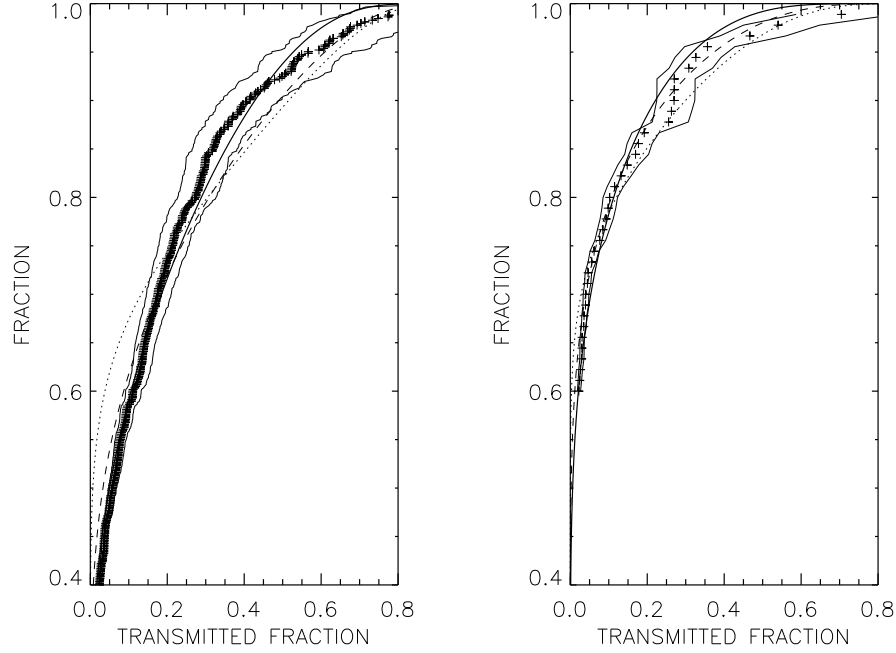


FIG. 10.— A comparison of the observed cumulative distribution function at  $z = 5.2$  (left panel) and at  $z = 5.7$  (right panel) with models in which  $g$  is constant and equal to the mean value given in Figure 9, and alternate models in which there is variation in  $g$  about the mean. At  $z = 5.2$ , the dashed line shows a model where half the points have  $g = 0.5$  and the other half have  $g = 1.8$ . The dotted line shows the case where half have  $g = 0.25$  and half have  $g = 1.9$ . For  $z = 5.7$ , the dashed line corresponds to a similar equal split between  $g = 0.4$  and  $g = 1.4$ , and the dashed line an equal split between  $g = 0.2$  and  $g = 1.6$ .

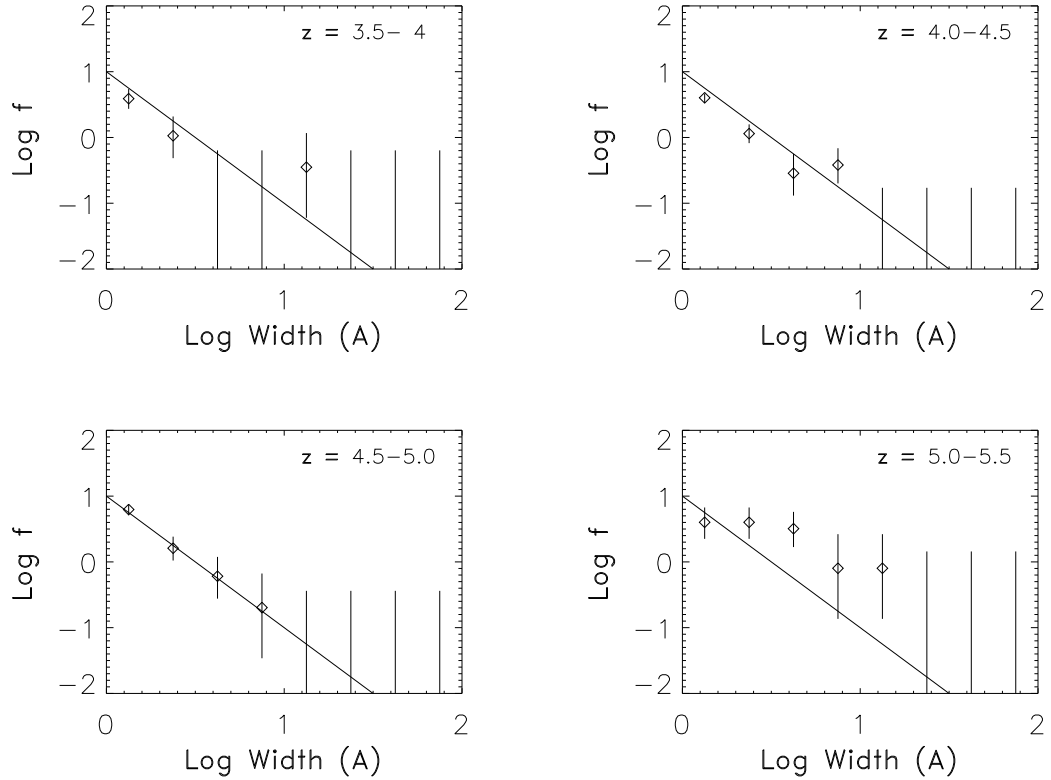


FIG. 11.— Distribution of the rest-frame widths, in Angstroms, of 'gaps' with optical depth  $> 2.5$  between  $1050 \text{ \AA}$  and  $1200 \text{ \AA}$  (rest-frame) for the quasar sample of pthis paper (excluding the Becker et al. sample).  $f$  is the number of gaps in each bin per unit redshift path. The bin size is  $10^{0.25}$  and the error bars are  $\pm 1\sigma$  based on the number of points in each bin. The solid line is a fiducial power law fitted to the  $z = 4.5 - 5$  distribution.

## 6. METAL LINES

At  $z < 4.5$  the mean metal content of damped Lyman alpha systems (DLAs) varies only slowly (Prochaska, Gawiser & Wolfe 2001) and, while there is a substantial dispersion in metallicity, all systems generally have metals with a minimum metallicity relative to solar of  $\sim 2 \times 10^{-3}$ . Since we can measure C II lines to column densities of  $\sim 10^{13} \text{ cm}^{-2}$  even in spectra with S/N similar to that of SDSS 1044–0125, if these metallicities were maintained to higher redshift we should be able to detect metal absorption to high column density neutral regions with  $N(\text{H I}) \geq 10^{19} \text{ cm}^{-2}$  and study the kinematic structure and velocity distribution of the gas.

Motivated by this idea, we have taken the list of ‘dark gaps’ with rest-frame Ly $\alpha$  widths  $> 4 \text{ \AA}$  from the sample developed in the previous section (Table 3) and searched at each position for associated metal lines. For each system we show in Figure 12 the Ly $\alpha$  profile and the corresponding lines of C II (1334  $\text{\AA}$ ), C IV (1548  $\text{\AA}$ ), Si II (1526  $\text{\AA}$ ), and Si IV (1393  $\text{\AA}$ ). The longer wavelength member of the C IV doublet at 1550  $\text{\AA}$  can also be seen. At  $z < 5$ , all of the gaps chosen in this way correspond to conventional DLAs whose Lyman series profiles can be fitted to the damping wings to obtain  $N(\text{H I})$ . The accuracy of the measurements is about 0.2 dex and where there are previous measurements of the same system (Prochaska et al. 2001 and references therein) the measured values agree at this level. We summarize these results in Table 3. At higher redshift ( $z > 5$ ) the line blending makes this type of measurement extremely difficult. For the  $z = 5.286$  system in SDSS 1044–0125 we measure an approximate  $\log N(\text{H I}) \sim 20.5$  from Ly $\alpha$  and Ly $\beta$ . The  $z = 5.397$  dark region has unsaturated regions at Ly $\beta$  and clearly has a lower column density. For the remaining two  $z > 5$  systems, we give upper limits on the column density based on the Ly $\alpha$  and Ly $\beta$  widths with  $\tau > 2.5$  using the equations of section (2).

For each region we have also measured the column density of Fe II, usually based on the 1608  $\text{\AA}$  line, and used this to obtain the value of [Fe/H]. No metal lines are seen in the three highest redshift systems. These results are also summarized in Table 3.

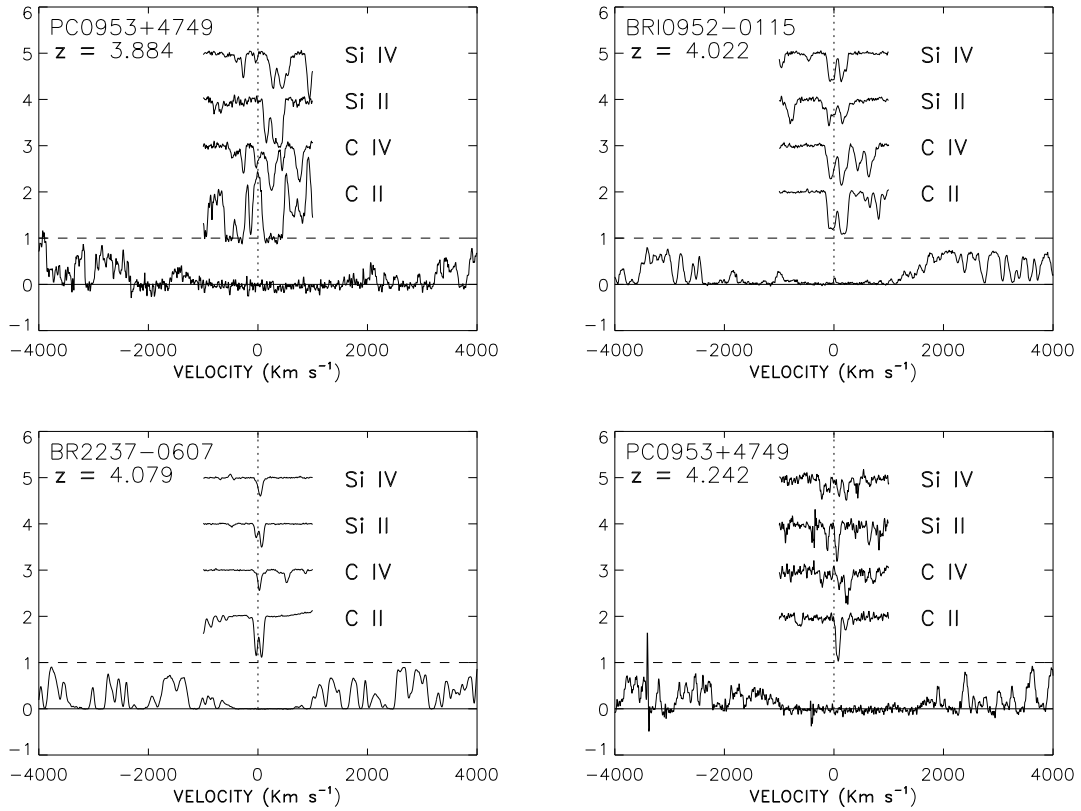


FIG. 12A.— Profiles of the absorption at Ly $\alpha$ , C II(1334  $\text{\AA}$ ), C IV(1548  $\text{\AA}$ ), Si II(1526  $\text{\AA}$ ), and Si IV(1393  $\text{\AA}$ ) for the sample of Table 3. The longer wavelength C IV(1550  $\text{\AA}$ ) and C II\*(1335  $\text{\AA}$ ) can also be seen in the C IV and C II profiles, respectively. The strong features seen at the C II position in SDSS 1737+5828 correspond to a lower redshift C IV doublet.

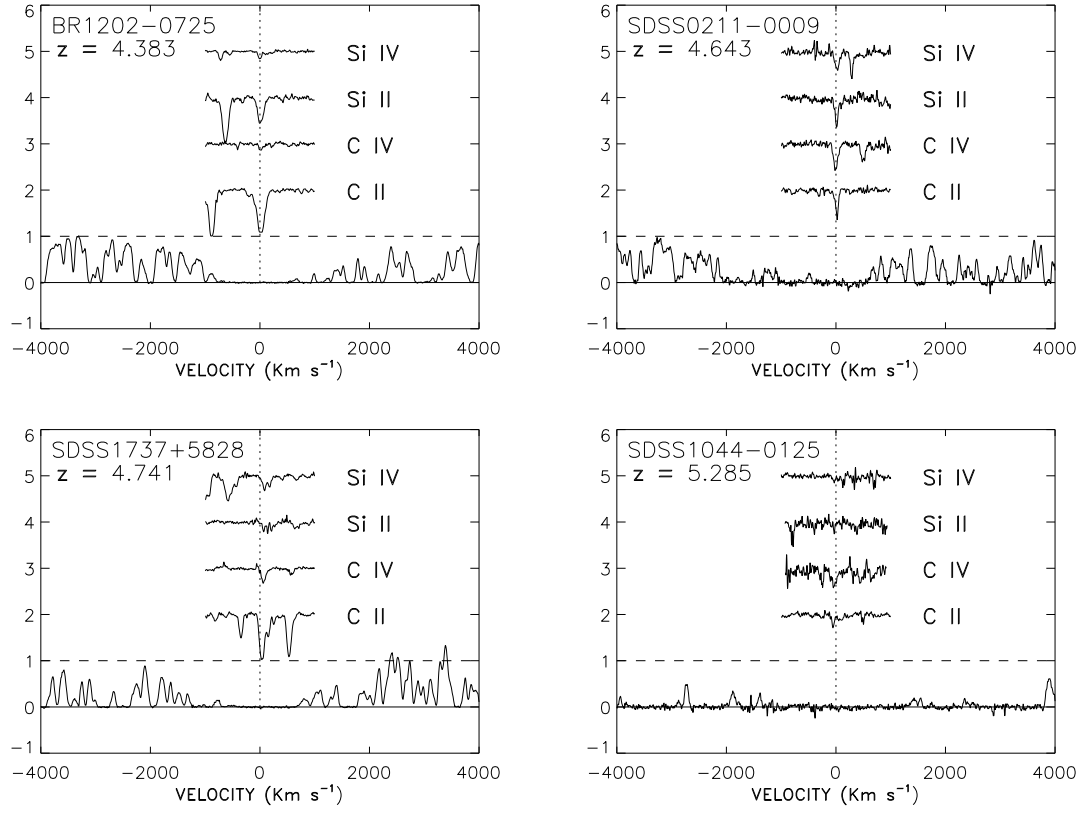


FIG. 12B.— Contd.

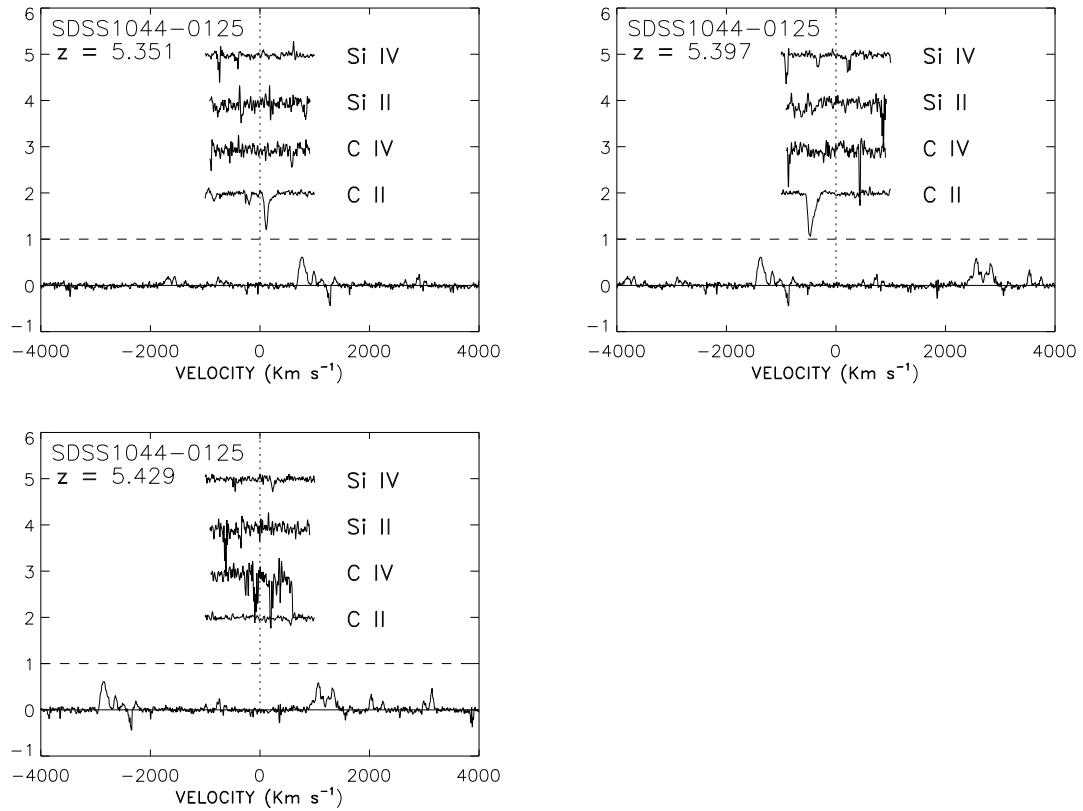


FIG. 12C.— Contd.

In Figure 13 we show  $[\text{Fe}/\text{H}]$  versus redshift (filled symbols) and we have also shown the lower redshift measurements summarized in Prochaska et al. (2001; open symbols). Three of our measurements overlap with these previous results, only one of which deviates by more than 0.2 dex: the present measurement of the  $z = 4.383$  system in BR 1202–0725 is 0.3 dex higher than that of Lu et al. (1996) which was, however, quite uncertain because of limited line coverage. The present measurement should be more accurate. From Figure 13 we can see that at these higher redshifts there is strong evidence that the metallicity is beginning to fall. The median metallicity at  $z < 4$  is  $-1.77$  and only one of the 12 systems above  $z = 4$  has a metallicity higher than this. The median metallicity of the 9 systems with  $4 < z < 4.5$  is  $-1.94$  and for the 3 systems with  $z > 4.5$  it is  $-2.61$ . If this trend continues to higher redshift, many of the stronger neutral hydrogen systems may not be seen in the metals and the systems that are seen may be somewhat too weak for study of the kinematics. However, even allowing for these low metallicities, which result in weak lines not being seen, Figure 12 shows that these systems are kinematically very simple at the higher redshifts. All of the three metal systems at  $z > 4.5$  are strongly dominated by a single narrow component. In each case we have measured  $b$ -values using the strongest unsaturated line of C II or Si II available, obtaining  $b = 19 \text{ km s}^{-1}$  at  $z = 4.64357$ ,  $b = 19 \text{ km s}^{-1}$  at  $z = 4.74314$  in SDSS 1737+5828, and  $b = 15 \text{ km s}^{-1}$  at  $z = 5.28538$  in SDSS 1044–0125. Taking into account the broad instrumental profile, these  $b$ -values might best be treated as upper limits, but irrespective of this point, it is clear that the high- $z$  DLAs are arising in kinematically quiescent regions, with line-of-sight turbulent velocity dispersions of less than  $10 - 14 \text{ km s}^{-1}$ .

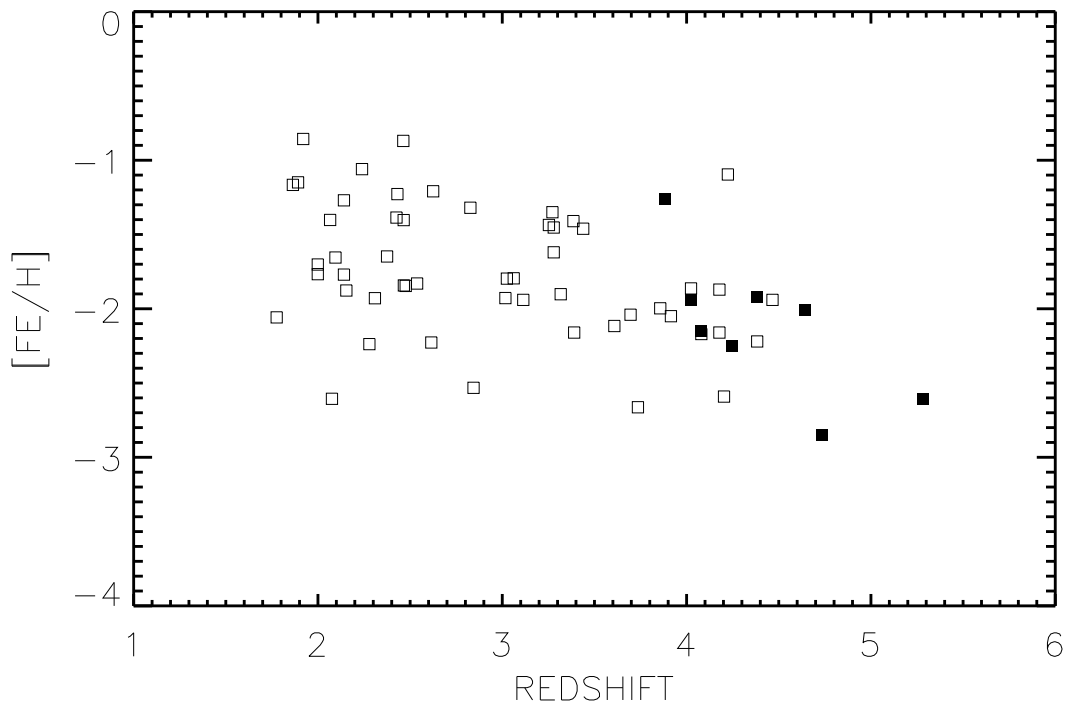


FIG. 13.— The metallicity relative to solar, based on the ratio of Fe II to H I column densities. The filled symbols show the present measurements and the open symbols, the values summarized in Prochaska, Gawiser & Wolfe (2001). Three of the points (at  $z = 4.024$ ,  $4.080$  and  $4.383$ ) overlap between the two samples. The present value at  $z = 4.383$  is higher than the value in Prochaska et al. (see text).

## 7. CONCLUSIONS

The primary result of the present paper is that between redshifts 4 and 6 the Ly $\alpha$  forest smoothly evolves from its behaviour at lower redshifts. The presence of substantial 'dark gaps' in the Ly $\alpha$  forest region is a natural consequence of the increase in the gas density and the decrease in the amplitude of density fluctuations and there are no signatures which require us to lie in the immediate post-reionization universe at this epoch. Over this redshift range, the data are consistent with a constant ionization while, even comparing with values measured at lower redshifts (e.g. McDonald et al. 2000), the ionization rate at  $z = 5$  is still 40% of that at  $z = 3$ . This in turn implies production rates of ionizing photons which, extrapolated, could easily ionize the intergalactic gas to much higher redshifts.

The one possibly compelling piece of evidence for the onset of reionization just beyond  $z = 6$  is the wide very dark region seen at  $z = 6.05$  by Becker et al. (2001) in the spectrum of SDSS 1030+0524. The present data are consistent with the LCDM model used by Cen & McDonald (2001) to show that, at the  $2 \sigma$  confidence level, the ionization rate at this point must have dropped by a factor of 2 from that at a redshift just less than 6. However, the data are also consistent with models in which there is a large variation in the ionization parameter about the mean at any given redshift, and in

this case the probability of seeing such a point becomes high enough to be consistent with the extrapolation from lower redshift. We have also noted that 2 out of the 15 quasars show BAL QSO behaviour and that this results in a substantial increase in the Ly $\alpha$  opacity near the quasar.

Finally, we have measured the metallicity of the gas in the damped Ly $\alpha$  systems in the quasars and show that the metallicity in these systems is beginning to drop at  $z = 5$ . The kinematic structure of the metal lines shows that, at these redshifts, the neutral hydrogen arises in single rather narrow regions with line-of-sight velocity dispersions of  $10 - 14 \text{ km s}^{-1}$ .

We would like to thank Patrick McDonald, Renyue Cen, Xiaohui Fan and Bob Becker for supplying tabular versions of data from their papers and/or their numerical models, and Patrick McDonald, Michael Strauss and Julia Kennefick for very useful comments on the text. This research was supported by the National Science Foundation under grants AST 96-17216 and AST 00-98480.

## REFERENCES

- Barkana, R. 2001, preprint (astro-ph/0108431).  
 Becker, R. H., et al. 2001, AJ, in press (astro-ph/0108097).  
 Cen, R. & McDonald, P. 2001, ApJL, submitted (astro-ph/0110306).  
 Croft, R. A. C. 1998, in Eighteenth Texas Symposium on Relativistic Astrophysics and Cosmology, Olinto, A. V., Frieman, J. A. & Schramm, D. N. eds., (River Edge, N. J. : World Scientific) , p. 664.  
 Djorgovski, S. G., Castro, S. M., Stern, D. & Mahabel, A. A. 2001, preprint (astro-ph/0108069).  
 Fan, X. et al. 2001a, AJ, in press (astro-ph/0108063).  
 Fan, X. et al. 2001b, AJ, submitted (astro-ph/0111184).  
 Goodrich, R. W. et al. 2001, ApJL, in press (astro-ph/0109464).  
 Gunn, J. E., & Peterson, B. A. 1965, ApJ, 142, 1633.  
 Hu, E. M., Kim, T.-S., Cowie, L. L., Songaila, A. & Rauch, M. 1995, AJ, 110, 1526.  
 Hu, E. M. et al. 2001, in preparation.  
 Hui, L. & Gnedin, N. Y. 1997, MNRAS, 292, 27.  
 Kennefick, J. D., Djorgovski, G. & De Carvalho, R. R. 1995, AJ, 110, 2553.  
 Kim, T.-S., Hu, E. M., Cowie, L. L. & Songaila, A. 1997, AJ, 114, 1.  
 Kirkman, D. & Tytler, D. 1997, ApJ, 484, 672.  
 Lu, L., Sargent, W. L. W., Barlow, T. A., Churchill, C. W. & Vogt, S. S. 1996, ApJS, 107, 475.  
 Madau, P., Haardt, F. & Rees, M. J. 1999, ApJ, 514, 648.  
 McDonald, P. & Miralda-Escudé, J. 2001, ApJ, 549, L11.  
 McDonald, P. et al. 2000, ApJ, 543, 1.  
 Miralda-Escudé, J., Cen, R., Ostriker, J. P. & Rauch, M. 1996, ApJ, 471, 582.  
 Miralda-Escudé, J., Haehnelt, M. & Rees, M. J. 2000, ApJ, 530, 1.  
 Oke, J. B. & Korycansky, D. G. 1982, ApJ, 255, 11.  
 Pentericci, L., et al. 2001, AJ, submitted [astro-ph/0112075]  
 Prochaska, J. X. et al. 2001, ApJS, 137, 21.  
 Prochaska, J. X., Gawiser, E. & Wolfe, A. M. 2001, ApJ, 552, 99.  
 Rauch, M., Miralda-Escudé, J., Sargent, W. L. W., Barlow, T. A., Weinberg, D. H., Hernquist, L., Katz, N., Cen, R., Ostriker, J. P. 1997, ApJ, 489, 7.  
 Razoumov, A. O., Norman, M. L., Abel, T. & Scott, D. 2001, preprint (astro-ph/0109111).  
 Scheuer, P. A. G. 1965, Nature, 207, 963.  
 Schneider, D. P., Schmidt, M. & Gunn, J. E. 1991, AJ, 101, 2004.  
 Sheinis, A. I., Miller, J. S., Bolte, M. & Sutin, B. M. 2000, Proc. SPIE, 4008, 522.  
 Shklovskij, I. S. 1964, Astron. Tsirkulyar, AN SSR, 3, 303.  
 Songaila, A., Hu, E. M., Cowie, L. L. & McMahon, R. G. 1999, ApJ, 525, L5.  
 Zhang, Y., Anninos, P., Norman, M. L. & Meiksin, A. 1997, ApJ, 485, 496.

TABLE 1  
OBSERVATIONS

Quasar	Mag.	Expo. (hrs)	$z_{em}$
SDSS 0211-0009	20.0	6.0	4.90
SDSS 0231-0728	19.2	3.0	5.42
SDSS 0338+0021	20.0	7.25	5.01
BRI 0952-0115	18.7	4.25	4.42
BR 1033-0327	18.5	2.0	4.51
SDSS 1044-0125	19.7	5.75	5.74
SDSS 1204-0021	19.1	3.0	5.07
BR 1202-0725	18.7	3.0	4.61
SDSS 1321+0038	20.1	2.0	4.71
SDSS 1605-0122	19.4	3.75	4.93
WFSJ 1612+5255	19.9	1.5	4.95
SDSS 1737+5828	19.3	7.5	4.85
SDSS 2200+0017	19.1	5.3	4.78
SDSS 2216+0013	20.3	3.0	5.00
BR 2237-0607	18.3	11.6	4.55



TABLE 2  
MEAN TRANSMISSIONS

$\langle z \rangle$	# points	$\langle F \rangle$	$\sigma$	$\sigma_{\text{mean}}$
4.09	15	0.352	0.103	0.027
4.34	20	0.334	0.088	0.020
4.61	15	0.260	0.065	0.017
4.93	5	0.162	0.049	0.022
5.20	8	0.107	0.063	0.022
5.51	7	0.074	0.028	0.011

TABLE 3  
DLA  $\text{Ly}\alpha$  WIDTHS, COLUMN DENSITIES AND METALLICITIES

Quasar	$z_{\text{abs}}$	$dW(\text{Ly}\alpha)^{(\text{a})}$	$z_{\text{metal}}$	$N(\text{H I})$	$N(\text{Fe II})$	[Fe/H]
SDSS 1044–0125	5.429	6.3	0.0	< 20.70	0.00	0.00
SDSS 1044–0125	5.397	5.6	0.0	0.00	0.00	0.00
SDSS 1044–0125	5.351	5.3	0.0	< 20.55	0.00	0.00
SDSS 1044–0125	5.286	10.3	5.284	(20.50)	13.34	(−2.65)
SDSS 1737+5828	4.742	5.9	4.743	20.65	13.30	−2.85
SDSS 0211–0009	4.643	4.1	4.644	20.00	13.49	−2.00
BR 1202–0725	4.383	6.9	4.384	20.60	14.09	−2.00
PC 0953+4749	4.243	8.0	4.244	20.70	13.95	−2.25
BR 2237–0607	4.079	5.6	4.080	20.55	13.88	−2.15
BRI 0952–0115	4.023	7.9	4.023	20.65	14.21	−1.95
PC 0953+4749	3.884	9.8	3.883	20.85	15.09	−1.25

<sup>(a)</sup>Rest-frame  $\text{Ly}\alpha$  width for  $\tau > 2.5$ .